

# Parallelization Techniques for Verifying Neural Networks

Haoze Wu<sup>1</sup>, Alex Ozdemir<sup>1</sup>, Aleksandar Zeljić<sup>1</sup>, Ahmed Irfan<sup>1</sup>, Kyle Julian<sup>1</sup>,  
 Divya Gopinath<sup>2</sup>, Sajjad Fouladi<sup>1</sup>, Guy Katz<sup>5</sup>, Corina Pasareanu<sup>3,4</sup>, and  
 Clark Barrett<sup>1</sup>

<sup>1</sup> Stanford University, USA

<sup>2</sup> NASA Ames, KBR Inc.

<sup>3</sup> NASA Ames, Moffett Field, CA

<sup>4</sup> Carnegie Mellon University, USA

<sup>5</sup> The Hebrew University of Jerusalem, Israel

**Abstract.** Inspired by recent successes with parallel optimization techniques for solving Boolean satisfiability, we investigate a set of strategies and heuristics that aim to leverage parallel computing to improve the scalability of neural network verification. We introduce an algorithm based on partitioning the verification problem in an iterative manner and explore two partitioning strategies, that work by partitioning the input space or by case-splitting on the phases of the neuron activations, respectively. We also introduce a highly parallelizable pre-processing algorithm that can be used to simplify neural network verification problems. An extensive experimental evaluation shows the benefit of these techniques on both existing benchmarks and new benchmarks from the aviation domain. A preliminary experiment with ultra-scaling our algorithm using a large distributed cloud-based platform also shows promising results.

## 1 Introduction

Recent breakthroughs in machine learning, specifically the rise of *deep neural networks (DNNs)* [7], have expanded the horizon of real-world problems that can be tackled effectively. Increasingly, complex systems are created using machine learning models [13] instead of using conventional engineering approaches. Machine learning models are trained on a set of labeled examples, using algorithms that allow the model to capture their properties and generalize them to unseen inputs. In practice, deep neural networks can significantly outperform hand-crafted systems, especially in fields where precise problem formulation is challenging, such as image classification [17], speech recognition [12] and game playing [27].

Despite their overall success, the black-box nature of DNNs calls into question their trustworthiness and hinders their application in safety-critical domains. These limitations are exacerbated by the fact that DNNs are known to be vulnerable to *adversarial perturbations*, small modifications to the inputs that lead to wrong responses from the network [28], and real-world attacks have already been carried out against safety-critical deployments of DNNs [2, 19]. One promising approach for addressing these concerns is the use of formal methods to certify and/or obtain rigorous guarantees about DNN behavior.

Early work in DNN formal verification [24, 25] focused on translating DNNs and their properties into formats supported by existing verification tools like general-purpose *Satisfiability Modulo Theories* (SMT) solvers (e.g., Z3 [3], CVC4 [1]). However, this approach was limited to small toy networks (roughly tens of nodes).

More recently, a number of DNN-specific approaches and solvers, including Reluplex [14], ReluVal [30], Planet [4], and Marabou [16], have been proposed and developed. These techniques scale to hundreds or a few thousand nodes. While a significant improvement, this is still several orders of magnitude fewer than the the number of nodes present in many real-world applications. Scalability thus continues to be a challenge and the subject of active research.

Inspired by recent successes with parallelizing SAT solvers [9, 11], we propose a set of strategies and heuristics for leveraging parallelism to improve the scalability of neural network verification. The paper makes the following contributions:

1. We propose a divide-and-conquer algorithm for neural network verification that is parameterized by different partition strategies and constraint solvers (Sec. 3);
2. We describe two partitioning strategies for this algorithm (Sec. 3.1): one that works by partitioning the input domain and a second one that performs case splitting based on the activation functions in the neural network;
3. We introduce the notion of *polarity* and use it to refine the partitioning (Sec. 3.2);
4. We introduce a highly parallel pre-processing algorithm that significantly simplifies verification problems (Sec. 3.3);
5. We show how polarity can additionally be used to speed up satisfiable queries (Sec. 3.4); and
6. We perform an extensive experimental evaluation on existing and new neural network verification benchmarks from the aviation domain, and we perform an *ultra-scalability* experiment using cloud computing (Sec. 4).

We begin with preliminaries, review related work in Sec. 5, and conclude in Sec. 6.

## 2 Preliminaries

In this section, we briefly review neural networks and their formalization, as well as the Reluplex algorithm for verification of neural networks.

### 2.1 Formalizing Neural Networks

**Deep Neural Networks.** A feed-forward *Deep Neural Network* (DNN) consists of a sequence of layers, including an input layer, an output layer, and one or more hidden layers in between. Each hidden layer consists of multiple *neurons*, whose values can be computed based on outputs from the preceding layer. Given an assignment of values to inputs, then, the output of the DNN can be computed by iteratively computing the values for neurons in each layer. Typically, a neuron’s assignment is determined by computing a linear transformation of the outputs of the neurons in the previous layer and then applying a non-linear function, known as an *activation function*. A popular activation function is the Rectified Linear Unit (ReLU), which is defined as  $\text{ReLU}(x) = \max(0, x)$  (see [18, 20, 22]). In this paper,

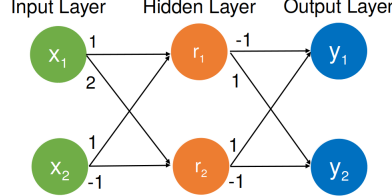


Fig. 1: A small feed-forward DNN  $\mathcal{N}$ .

we focus on DNNs with ReLU activation functions, and we assume that the output of each neuron is computed as  $\text{ReLU}(w_1 \cdot v_1 + \dots + w_n \cdot v_n + b)$  where  $v_1 \dots v_n$  are the values of the neurons from the previous layer,  $w_1 \dots w_n$  are the weight parameters and  $b$  is a bias parameter associated with the neuron. A neuron is *active* or in the *active phase*, if its input is positive; otherwise, it is *inactive* or in the *inactive phase*.

We use a simple feed-forward ReLU DNN  $\mathcal{N}$ , shown in Fig. 1, as a running example throughout this paper. The network has two inputs (denoted  $x_1$  and  $x_2$ ) and two outputs (denoted  $y_1$  and  $y_2$ ) in the input and output layers, respectively. The network has one hidden layer, whose neurons (denoted  $r_1$  and  $r_2$ ) use the ReLU activation function. The weights are written on the edges. For simplicity, all biases are 0. Consider the input  $\langle x_1, x_2 \rangle = \langle -1, 2 \rangle$ . The output of  $\mathcal{N}$  on this input is  $\langle -1, 1 \rangle$ . To see this, notice that the output of the hidden layer is  $\langle \text{ReLU}(1 \cdot (-1) + 1 \cdot 2), \text{ReLU}(2 \cdot (-1) + (-1) \cdot 2) \rangle = \langle 1, 0 \rangle$ . This feeds into the output layer, which computes  $\langle y_1, y_2 \rangle = \langle (-1) \cdot 1 + 1 \cdot 0, 1 \cdot 1 + (-1) \cdot 0 \rangle = \langle -1, 1 \rangle$ . In this case,  $r_1$  is active, and  $r_2$  is inactive. A feed-forward DNN is called *fully-connected* if all neurons in a hidden layer feed into all neurons in the next layer— $\mathcal{N}$  is such a network.

**Verification of Neural Networks.** A neural network verification problem consists of two components: a neural network  $N$ , and a property  $P$ .  $P$  is often of the form  $P_{in} \Rightarrow P_{out}$ , where  $P_{in}$  is a formula over the inputs of  $N$  and  $P_{out}$  is a formula over the outputs of  $N$ . Typically,  $P_{in}$  defines an input region  $I$  for the input layer and  $P$  states that for each point in  $I$ ,  $P_{out}$  holds for the output layer. Given a query like this, a verification tool tries to find a counter-example: an input point  $i$  in  $I$ , such that when applied to  $N$ ,  $P_{out}$  is false over the resulting outputs.  $P$  holds only if such a counter-example does not exist.

The property to be verified may arise from the specific domain where the network is deployed. For instance, for networks that are used as controllers in an unmanned aircraft collision avoidance system (e.g., the ACAS Xu networks [14]), we would expect them to produce sensible advisories according to the location and the speed of the intruder planes in the vicinity. On the other hand, there are also properties that are generally desirable for a neural network. One such property is *local adversarial robustness* [15], which states that a small norm-bounded input perturbation should not cause major spikes in the network's output.

**Definition 1.** A DNN  $N$  is  $(\delta, \epsilon)$ -locally robust at input point  $x$ , iff

$$\forall x', \|x - x'\| \leq \delta \Rightarrow N(x) - N(x') \leq \epsilon.$$

More generally, a property may be an arbitrary formula over input values, output values, and values of hidden layers—such problems arise for example in

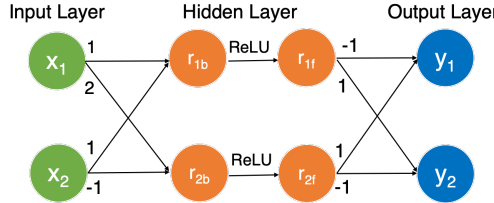


Fig. 2: The network from Fig. 1, with ReLU nodes split into two variables.

the investigation of the neural networks' explainability [8], where one wants to check whether the activation of a certain ReLU  $r$  implies a certain output behavior (e.g., the neural network always predicts a certain class). The verification of neural networks with ReLU functions is decidable and NP-Complete [14]. As with many other verification problems, scalability is a key challenge.

**VNN Formulas.** We introduce the notion of VNN (Verification of Neural Network) formulas to formalize Neural Network verification queries. Let  $\mathcal{X}$  be a set of variables. A *linear constraint* is of the form  $\sum_{x_i \in \mathcal{X}} a_i x_i \bowtie b$ , where  $a_i, b$  are rational constants, and  $\bowtie \in \{\leq, \geq, =\}$ . A *ReLU constraint* is of the form  $\text{ReLU}(x_i) = x_j$ , where  $x_i, x_j \in \mathcal{X}$ . A *VNN formula*  $\phi$  is a conjunction of linear constraints and ReLU constraints. A feed-forward neural network can be encoded as a VNN formula. The trick is to use a pair of variables  $r_b, r_f$  for each ReLU  $r$  to encode it as a ReLU constraint and to encode the weighted sums as linear constraints. We refer to the  $r_b$  variables as *backward-facing variables*, and they are used to connect  $r$  to the preceding layer. The  $r_f$  are called *forward-facing variables* and are used to connect  $r$  to the next layer. Consider again the network  $\mathcal{N}$ , shown in Fig. 2, with two variables for each hidden node.  $\mathcal{N}$  can now be encoded as the formula  $\phi_{\mathcal{N}}$  which we define as the conjunction of the following linear and ReLU constraints.

$$\begin{aligned} r_{1b} - x_1 - x_2 &= 0 & r_{2b} - 2x_1 + x_2 &= 0 & y_1 + r_{1f} - r_{2f} &= 0 \\ y_2 - r_{1f} + r_{2f} &= 0 & \text{ReLU}(r_{1b}) &= r_{1f} & \text{ReLU}(r_{2b}) &= r_{2f} \end{aligned}$$

In general, a property could be any formula  $P$  over the variables used to represent  $\mathcal{N}$ . To check whether  $P$  holds on  $\mathcal{N}$ , we simply conjoin the representation of  $\mathcal{N}$  with the negation of  $P$  and use a constraint solver to check for satisfiability.  $P$  holds iff the constraint is unsatisfiable. Suppose, for example, that we have a property  $P_0$  given by:

$$(-2 \leq x_1 \leq 1 \wedge -2 \leq x_2 \leq 2) \Rightarrow y_1 > y_2 \quad (1)$$

Checking this property on  $\mathcal{N}$  amounts to checking the satisfiability of the VNN formula  $\phi = \phi_{\mathcal{N}} \wedge \neg P_0$ :

$$\phi = \phi_{\mathcal{N}} \wedge (-2 \leq x_1 \leq 1) \wedge (-2 \leq x_2 \leq 2) \wedge (y_1 \leq y_2), \quad (2)$$

Note that a solver for VNN formulas can solve a property  $P$  only if the negation of  $P$  is also a VNN formula. We assume this is the case in this paper, but more general properties can be handled by decomposing  $\neg P$  into a disjunction of VNN formulas and checking each separately (or, equivalently, using a DPLL( $T$ ) approach [23]). This works as long as the atomic constraints are linear. Non-linear constraints (other than ReLU) are beyond the scope of this paper.

$$\begin{array}{c}
\text{Simplex } \frac{x \in X \quad A(x) < L(x) \vee A(x) > U(x)}{S := \text{Simplex}(S)} \\
\text{Sat } \frac{\forall x \in X. L(x) \leq A(x) \leq U(x) \quad \forall \langle x, y \rangle \in R. A(y) = \text{ReLU}(A(x))}{\text{SAT}} \\
\text{Relu-F } \frac{\langle x, y \rangle \in R \quad A(y) \neq \text{ReLU}(A(x))}{A := A[y \mapsto \text{ReLU}(A(x))]} \quad \text{Relu-B } \frac{\langle x, y \rangle \in R \quad A(y) \neq \text{ReLU}(A(x)) \quad A(y) \geq 0}{A := A[x \mapsto A(y)]} \\
\text{Split } \frac{\langle x, y \rangle \in R \quad L(x) < 0 \quad U(x) > 0}{u(x) := 0, E := E \cup \{y = 0\} \quad l(x) := 0, E := E \cup \{x = y\}}
\end{array}$$

Fig. 3: Transition rules for the Reluplex algorithm

## 2.2 The Reluplex Procedure

The Reluplex procedure [14] is a sound and complete algorithm that decides the satisfiability of a VNN formula. The procedure extends the Simplex algorithm—a standard efficient decision procedure for conjunctions of linear constraints—to handle ReLU constraints. At a high level, the algorithm iteratively searches for an assignment that satisfies all the linear constraints, but treats the ReLU constraints lazily in the hope that many of them will be irrelevant for proving the property.

In [14], the Reluplex procedure is presented as an abstract calculus. We present a condensed version of it here. Formally, the procedure operates on a data structure called a *configuration*. For a given set of variables  $X$ , a configuration  $S$  is either one of the distinguished symbols  $\{\text{SAT}, \text{UNSAT}\}$ , or a tuple  $\{E, R, L, U, A\}$ , where:  $E$  is a set of linear equality constraints, whose variables are in  $X$ ;  $R \subseteq X \times X$  denotes a set of ReLU constraints; and  $L, U$ , and  $A$  are functions from  $X$  to  $\mathbb{R}$  that map each variable to a lower bound, upper bound, and current value, respectively. A VNN formula  $\phi$  can be translated into a configuration  $S$  as follows: each ReLU constraint  $\text{ReLU}(x) = y$  is added as a pair  $\langle x, y \rangle$  to  $R$ ; for each linear constraint  $\sum_{x_i \in X} c_i x_i \bowtie b$ , a fresh variable  $y$  is introduced, the equation  $y = \sum_{x_i \in X} c_i x_i$  is added to  $E$ , and  $b$  is added as a bound for  $y$  (either upper, lower, or both, depending on  $\bowtie$ ). The assignment  $A$  is initially set to 0 for all variables, ensuring that all equations in  $E$  hold (though variable bounds and ReLU constraints may be violated). The Reluplex procedure decides the satisfiability of  $\phi$  by repeatedly applying *transformation rules* to  $S$  until  $\text{SAT}$  is derived or all branches end in  $\text{UNSAT}$ . The rules are given in *guarded assignment form*, where the top of the rule describes the conditions under which the rule can be applied, and the bottom of the rule describes how the configuration is modified when the rule is applied.

The rules are shown in Figure 3. The *Simplex* rule is simply an abstraction of the simplex procedure. It is applicable when some variable is not within its bounds. It calls *Simplex* on the current configuration. We assume that *Simplex* is some decision procedure which either returns the same configuration except with a new assignment in which all variables are within bounds or *UNSAT* if no such assignment exists (see [14] for a more detailed presentation of the Simplex algorithm). The *Sat* rule recognizes when all variables are within bounds and all ReLU constraints are satisfied and transitions to the *SAT* configuration. The *Relu-F* and *Relu-B* rules are applicable when some ReLU constraint is not satisfied. *Relu-F* simply updates the assignment for the forward-facing variable to the value obtained by applying the ReLU function to the value of the backward-facing variable. *Relu-B* fixes the

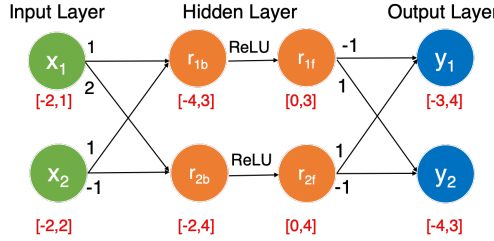


Fig. 4: Bounds of variables obtained by forward bound propagation.

constraint the other way, by setting the assignment for the backward-facing variable to be equal to that of the forward-facing variable. Note that *Relu-B* is only applicable when the forward-facing variable is non-negative. Finally, the *Split* rule is applicable to any ReLU constraint that could be active or inactive (i.e. the bounds on the backward-facing variable do not constrain it to be one or the other). It creates two cases, one for the active case and one for the inactive case.

The basic strategy (more details are in [14]) for using the rules in Figure 3 to solve a VNN formula is: 1) check whether *Sat* applies, and if so, terminate with a satisfiable result; 2) if *Simplex* is applicable, apply it; if the result is *UNSAT*, terminate with an unsatisfiable result; otherwise, go to step 1; 3) apply *Relu-F* or *Relu-B* and then go to step 1, unless these rules have already been applied to the broken ReLU constraint more than some threshold number of times; 4) apply the split rule and go to step 1. As shown in [14], the algorithm is sound, complete and terminating.

In this paper, we do a more focused exploration of two decision points highlighted by the above strategy. The first is the question of which rule to apply in step 3, *Relu-F* or *Relu-B* (often both are applicable). We refer to the strategy used to make this decision as the *direction heuristic*, and we discuss direction heuristics, especially in the context of parallel solving in Section 3.4. The other is the question of which ReLU constraint to choose in step 4. We refer to the strategy used for making this decision as the *branching heuristic*. We explore branching heuristics and their application to parallelizing the algorithm in Sections 3.1 and 3.2.

**Bound propagation.** The full *Reluplex* procedure also uses bound propagation to derive bounds for variables in hidden layers. As the search progresses, the lower and upper bounds of the variables in each layer are tightened, which in turn can trigger additional propagations and more bound tightening. This process is especially useful when it constrains a ReLU variable in such a way that the ReLU is forced into either the active or inactive state, thus reducing the search space [14]. Figure 4 shows the result of propagating bounds for property  $P_0$  (formula (1)) on the example from Fig. 2.

### 3 D&C: Parallelizing the Reluplex Procedure

In this section, we present a parallel algorithm called *Divide-and-Conquer* (or simply D&C) for solving VNN formulas, based on the *Reluplex* procedure and an

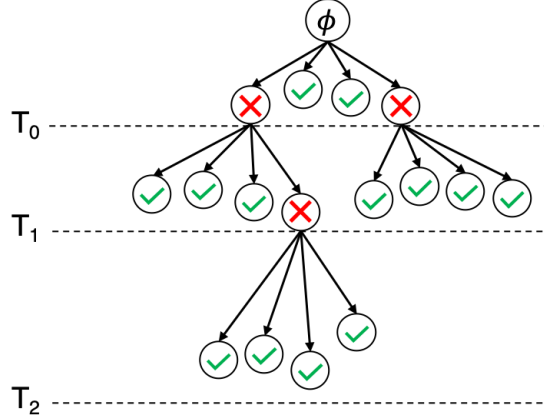


Fig. 5: An execution of the D&C algorithm.

iterative-deepening strategy. We then present two partitioning strategies: input-based<sup>6</sup> and ReLU-based.

The D&C algorithm partitions an input problem into several sub-problems (that are ideally easier to solve), and tries to solve each sub-problem within a given time budget. If solving a problem exceeds the time budget, that problem is further *partitioned* and the resulting sub-problems are allocated an *increased time budget*. Fig. 5 shows solving of problem  $\phi$  as a tree, where the root of the tree denotes the original problem. The sub-problems that exceed their allotted time are partitioned, becoming inner nodes, and every sub-problem that is solved within the allotted time budget is a leaf. Formula  $\phi$  is satisfiable if some leaf is satisfiable. Assuming the partitioning is *exhaustive*, that is:  $\phi = \bigvee_{\phi_i \in \text{partition}(\phi, n)} \phi_i$ , for any  $n > 1$ , then  $\phi$  is unsatisfiable iff all the leaves are unsatisfiable.

The D&C algorithm, shown in Algorithm 1, can be seen as a framework parameterized by the *partitioning heuristic* and the underlying *solver*. Details of these parameters are abstracted away within the **partition** and **solve** functions respectively and will be discussed in subsequent sections. The D&C algorithm takes as input a VNN formula  $\phi$  and the search shape parameters - initial number of partitions  $N_0$ , initial timeout  $T_0$ , number of partitions  $N$ , and the timeout factor  $F$ . During solving, D&C maintains a queue  $Q$  of  $\langle \text{query}, \text{timeout} \rangle$  pairs, which is initialized with an  $N_0$ -partition of the original query  $\phi$  and the initial timeout  $T_0$ . While the queue is not empty, the next query-timeout pair  $\langle \phi', t' \rangle$  is retrieved from the queue  $Q$ , and the query  $\phi'$  is solved with time budget  $t'$ . If  $\phi'$  is satisfiable, then the original query  $\phi$  is satisfiable, and **SAT** is returned. If  $\phi'$  times out, **partition**( $\phi', N$ ) creates  $N$  sub-problems of  $\phi'$ , which are put in the queue with the time budget  $t' \cdot F$ . If a sub-problem  $\phi'$  is unsatisfiable, no special action needs to be taken. If  $Q$  becomes empty, the original query is unsatisfiable and the algorithm returns **UNSAT**. The main loop of the algorithm naturally lends itself to parallelization, since the **solve** calls are mutually independent and query-timeout

<sup>6</sup> We note that an input-based strategy was briefly described in [16], although not many details were given.

---

**Algorithm 1** Divide-and-Conquer

---

**Input:** query  $\phi$ , initial partition size  $N_0$ , initial timeout  $T_0$ , partition size  $N$ , timeout factor  $F$   
**Output:** SAT/UNSAT

```
for  $\psi \in \text{partition}(\phi, N_0)$  do
     $Q.$  enqueue( $(\psi, T_0)$ )
    while  $Q.$  notEmpty() do
         $(\phi', t') \leftarrow Q.$  dequeue()
         $result \leftarrow \text{solve}(\phi', t')$ 
        if  $result = \text{SAT}$  then
            return SAT
        else if  $result = \text{TIMEOUT}$  then
            for  $\psi \in \text{partition}(\phi', N)$  do
                 $Q.$  enqueue( $(\psi, t' \cdot F)$ )
return UNSAT
```

---

pairs can be asynchronously enqueued and dequeued. We state without proof the following result, which is a well-known property of such algorithms.

**Theorem 1.** *The Divide-and-Conquer( $\phi, N_0, T_0, N, F$ ) algorithm is sound and complete if the following holds:*

1. the **solve** function is sound and complete; and
2. the **partition** function is exhaustive.

In addition, with modest assumptions on **solve** and **partition**, and with  $F > 1$ , it can be shown that the algorithm is also terminating. In particular, it is terminating for the instantiations we consider below. The D&C algorithm can be tailored to the available computing resources (e.g., number of processors) by specifying the number of initial splits  $N_0$ . The other three search parameters of D&C specify the dynamic behavior of the algorithm, e.g. if  $T_0$  and  $F$  are both small, or if the number of online partitions is large, then new sub-queries are created frequently, which entails a more aggressive D&C strategy (and vice versa). Notice that we can completely discard the dynamic aspect of D&C by setting the initial timeout to be  $\infty$ , which is the approach taken by [9] in the context of SAT solving.

A potential downside of the algorithm is that each call to **solve** that times out is essentially wasted time, overhead above and beyond the useful work needed to solve the problem. Fortunately, as the following theorem shows, the amount of time wasted can be mitigated by using a sufficiently large partition size.

**Theorem 2.** *If Algorithm 1 is called on an unsatisfiable formula and  $N \leq N_0$ , then the fraction of calls to **solve** that time out is at most  $\frac{1}{N}$ .*

*Proof.* Assume for the moment that  $N = N_0$ . We can view D&C's UNSAT proof as constructing an  $N$ -ary tree, as shown in Figure 5. The  $\ell$  leaf nodes correspond to calls to **solve** that do not time out. The  $t$  non-leaves are calls to **solve** that do time out. Since this is a tree, the total number of nodes,  $n = \ell + t$ , is one more than the number of edges. Since each query that times out has an edge to each of

its  $k$  sub-queries, the number of edges is  $Nt$ . Thus we have  $n = Nt + 1$  which can be rearranged to show the fraction of queries that time out:

$$\frac{t}{n} = \frac{1 - \frac{1}{n}}{N} \leq \frac{1}{N}$$

If  $N < N_0$ , then let  $k = N_0 - N$ . The number of nodes is then  $n = Nt + k + 1$ , and the result follows as before.  $\square$

Theorem 2 indicates that when  $N$  is sufficiently large, the extra time spent on internal nodes should be quite small compared to the total running time.

### 3.1 Partitioning Strategies

A partitioning strategy specifies how to break down a VNN formula  $\phi$  into smaller sub-problems. The goal of a partitioning is to produce smaller (and easier) problems. A ReLU is *fixed* when the bounds on the backward-facing or forward-facing variable either imply that the ReLU is active or imply that the ReLU is inactive. Fixing as many ReLUs as possible reduces the complexity of the resulting problem.

With this goal in mind, we present two strategies: 1. *input-based partitioning* creates case splits over the range of input variables and relies on bounds propagation to fix ReLUs, whereas 2. *ReLU-based partitioning* creates case splits that fix the phase of ReLUs directly. For soundness and completeness, it is crucial that the partitioning is exhaustive, which is the case for both strategies presented here. The *branching heuristic* which determines the choice of variable, respectively ReLU, on which to split, and properties like *balance*, the relative difficulty of resulting sub-problems, are very important for performance. To see the importance of balance, suppose the sub-formulas created by splitting ReLU<sub>1</sub> take 10 seconds and 300 seconds to solve, respectively, whereas those created by splitting ReLU<sub>2</sub> take 150 seconds and 160 seconds, respectively. While the total solving time is the same, the split on ReLU<sub>2</sub> will result in shorter wall-clock time, if we have two processors.

If most ReLUs in a DNN lead to easier and balanced sub-formulas, then D&C will perform well even without a carefully-designed branching heuristic. However, in practice we observe that often a significant portion of ReLUs result in greatly unbalanced sub-formulas: the solver can prove the unsatisfiability of one sub-formula quickly, while the other sub-formula takes just a little less time to solve than the original formula does. Therefore, an effective branching heuristic is crucial. We describe such heuristics below.

**Input-based Partitioning.** This simple partitioning strategy performs case splits over the range of an input variable. Consider again the encoding of a simple property on our example network given by the formula  $\phi$  in equation (2) from Section 2. Suppose we call **partition**( $\phi$ , 2) using the input-splitting strategy. There is a choice between two input variables  $x_1$  and  $x_2$ , and their input ranges are explicitly part of  $P$ . Assuming the function chooses variable  $x_1$ , with the aim of producing balanced sub-problems, the resulting set contains two formulas  $\phi_1$  and  $\phi_2$ :

$$\begin{aligned}\phi_1 &= \phi_N \wedge (-2 \leq x_1 < -0.5) \wedge (-2 \leq x_2 \leq 2) \wedge (y_1 \leq y_2), \\ \phi_2 &= \phi_N \wedge (-0.5 \leq x_1 \leq 1) \wedge (-2 \leq x_2 \leq 2) \wedge (y_1 \leq y_2).\end{aligned}$$

This partitioning is exhaustive since formulas  $\phi$  and  $\phi_1 \vee \phi_2$  are logically equivalent.

An obvious heuristic for this strategy is to choose the input whose bounds define the largest interval. A more sophisticated heuristic was introduced in [16]. Both of these heuristics perform reasonably well on benchmarks with few inputs (the ACAS Xu benchmarks, for example). Unfortunately, regardless of the heuristic used, this strategy suffers from the “curse of dimensionality”: with a large number of inputs it becomes increasingly difficult to fix ReLUs by splitting the input range of only one input variable. Thus, the input-partitioning strategy does not scale well on such networks (e.g., perception networks), which often have hundreds or thousands of inputs. In fact, partitioning the input region in such cases often leads to a set of sub-formulas that are not noticeably easier than the original formula.

**ReLU-based Partitioning.** Another strategy is to partition the search space by fixing ReLUs. This strategy can be viewed as an application of the `Split` rule shown in Fig. 3. Consider a VNN formula  $\phi = \phi' \wedge (\text{ReLU}(x) = y)$ . A call to `partition`( $\phi$ , 2) using the ReLU-based strategy results in two sub-formulas:

$$\begin{aligned}\phi_1 &= \phi' \wedge (\text{ReLU}(x) = y) \wedge (\mathbf{x} \leq \mathbf{0}) \wedge (\mathbf{y} = \mathbf{0}), \\ \phi_2 &= \phi' \wedge (\text{ReLU}(x) = y) \wedge (\mathbf{x} > \mathbf{0}) \wedge (\mathbf{x} = \mathbf{y}),\end{aligned}$$

where  $\phi_1$  captures the inactive and  $\phi_2$  the active phase of the ReLU. We next consider a heuristic for deciding which ReLU to choose.

### 3.2 Polarity-based Branching Heuristics

A recent successful approach to parallelizing Boolean satisfiability [11] guides the partitioning by estimating the difficulty of resulting sub-problems (by counting the number of unit propagations in the created sub-problems and using that to estimate how balanced the resulting problems are). In the context of VNNs, an obvious counterpart to unit-propagation is bound propagation. As a light-weight estimate of bound propagation, we propose a metric called *polarity*. Given a ReLU constraint,  $\text{ReLU}(x) = y$ , and bounds  $a \leq x \leq b$ , where  $a < 0$ , and  $b > 0$ , the polarity of the ReLU is:  $p = \frac{a+b}{b-a}$ . Polarity ranges from -1 to 1 and measures the symmetry of a ReLU’s bounds with respect to zero. For example, if we split on a ReLU constraint with polarity close to 1, the bound on the forward-facing variable in the active case,  $[0, b]$ , will be much wider than in the inactive case,  $[a, 0]$ . Intuitively, forward bound tightening would therefore result in tighter bounds in the inactive case. This means the inactive case will probably be much easier than the active case, so the partition is unbalanced and therefore undesirable. On the other hand, a ReLU with a polarity close to 0 is more likely to have balanced sub-problems. We also observe that ReLUs in early hidden layers are more likely to produce bound tightening by forward bound propagation (as there are more ReLUs that depend on those early ReLUs).

We thus propose a heuristic that picks the ReLU whose polarity is closest to 0 among the first  $k\%$  unfixed ReLUs, where  $k$  is a configurable parameter. Note that, in order to compute polarities, we need all input variables to be bounded.<sup>7</sup>

---

<sup>7</sup> This assumption is not too strong because even if the properties of interest do not impose additional constraints on the input region, reasonable bounds on each input dimension are typically known for a given DNN.

---

**Algorithm 2** Iterative Propagation

---

```
Input: VNN query  $\phi$ , timeout  $t$ 
Output: preprocessed query  $\phi'$ .
 $progress \leftarrow \top$ ;  $\phi' \leftarrow \phi$ 
while  $progress = \top$  do
     $progress \leftarrow \perp$ 
    for  $r$  in  $\text{getUnfixedReLUs}(\phi')$  do
         $\psi \leftarrow \text{PolarityConstraint}(r)$ 
         $result = \text{solve}(\phi' \wedge \psi, t)$ 
        if  $result = \text{UNSAT}$  then
             $\psi' \leftarrow \text{flipPhase}(\psi)$ 
             $\phi' \leftarrow \phi' \wedge \psi'$ 
             $progress \leftarrow \top$ 
    return  $\phi'$ 
```

---

To illustrate the ReLU-based partitioning strategy we just introduced, consider using it to partition formula (2) for our running example. The bounds for the backward-facing variables are shown in Figure 4. The estimated polarity of  $\text{ReLU}_1$  is  $\frac{-4+3}{3-(-4)} \approx -0.14$ , and the estimated polarity of  $\text{ReLU}_2$  is  $\frac{-2+4}{4-(-2)} \approx 0.33$ . Therefore, we would pick  $\text{ReLU}_1$  as the branching variable.

### 3.3 Fixing ReLU Constraints with Iterative Propagation

As discussed earlier, the performance of D&C depends heavily on being able to split on ReLUs that result in balanced sub-formulas. However, sometimes a significant portion of ReLUs in a given neural network cannot be split in this way. Fortunately, this opens up a separate opportunity for optimization that we take advantage of in a technique called *iterative propagation*, which is a preprocessing technique aimed at fixing ReLUs which lead to unbalanced partitions.

Concretely, for each ReLU in the VNN formula, we temporarily fix the ReLU to one of its phases and then attempt to solve the problem with a short timeout. The goal is to detect unbalanced and (hopefully) easy unsatisfiable cases. Pseudocode is presented in Algorithm 2. The algorithm takes as input a formula and a timeout  $t$ , and returns an equisatisfiable formula  $\phi'$  with potentially fewer unfixed ReLUs. The outer loop computes the fixed point, while the inner loop iterates through the as-of-yet unfixed ReLUs. For each unfixed ReLU, the `PolarityConstraint` function returns a constraint for the phase estimated to be easier using the polarity metric. If the solver returns `UNSAT`, then we can safely fix the ReLU to its other phase using the `flipPhase` function. We ignore the case where the solver returns `SAT`, since in practice this only occurs for formulas that are very easy in the first place.

Iterative propagation complements D&C, because the likelihood of finding balanced partitions is increased by fixing ReLUs that lead to unbalanced partitions. Moreover, iterative propagation is highly parallelizable, as each ReLU-fixing attempt can be solved independently. In this paper, we use iterative propagation as a preprocessing step, though it is possible to integrate the two processes even more closely, e.g., by performing iterative propagation after every `partition` call.

Again, there is a parallel with *unit propagation* in Boolean satisfiability, rooted in the Boolean nature of ReLUs and the principles behind conflict driven reasoning.

Unsurprisingly, there is a trade-off between the timeout  $t$  and the number of ReLUs fixed by iterative propagation, which we investigate in Section 4.

### 3.4 Speeding Up Satisfiable Checks with Polarity-Based Direction Heuristics

In this section we discuss how the polarity metric introduced in Section 3.2 can be used to solve satisfiable instances quickly. When splitting on a ReLU, the Reluplex algorithm faces the same choice as the D&C algorithm. For unsatisfiable cases, the order in which ReLU case splits are done make little difference on average, but for satisfiable instances, it can be very beneficial if the algorithm is able to hone in on a satisfiable sub-problem. We refer to the strategy for picking which ReLU phase to split on first as the *direction heuristic*.

We propose using the polarity metric to guide the direction heuristic for D&C. If the polarity of a branching ReLU is positive, then we process the active phase first; if the polarity is negative, we do the reverse. Intuitively, formulas with wider bounds are more likely to be satisfiable, and the polarity direction heuristic prefers the phase corresponding to wider bounds for the ReLU’s backward-facing variable.

Repairing broken ReLU constraints in the Reluplex procedure presents a similar decision, since there are two rules for fixing ReLU constraints (recall the description of the Reluplex procedure from Section 2). We extend our notion of direction heuristics to also apply to this decision: choosing which ReLU-fixing rule to use when both are applicable.

Following the same intuition as before, we propose to apply the rule that maximizes the width of the resulting bounds. For example, suppose the range of  $x$  is  $[-2, 1]$ ,  $A(x) = -1$  and  $A(y) = 1$ . We have the choice of either applying `Relu-F` to set  $y$  to 0 or applying `Relu-B` to set  $x$  to 1. In this case, the ReLU has negative polarity, indicating that the negative phase is associated with wider input bounds, so our heuristic applies the `Relu-F` rule.

Experimental results suggest that these direction heuristics improve performance on satisfiable instances. Interestingly, they also have a positive performance impact on unsatisfiable instances (see Section 4).

## 4 Experimental Evaluation

In this section, we evaluate the performance of the presented techniques on a diverse set of benchmarks from real-world applications, including safety properties of control systems as well as robustness properties of perception models.

### 4.1 Benchmarks

The benchmark set consists of network-property pairs, with networks from three different application domains: aircraft collision avoidance (ACAS Xu), aircraft localization (TaxiNet), and digit recognition (MNIST). Properties include robustness and domain-specific safety properties.

**ACAS Xu Family** The ACAS Xu family of VNN benchmarks was introduced in [14] and contains 45 fully-connected feed-forward neural networks, each with 5

hidden layers and 60 ReLU nodes per layer. The networks issue advisories to the controller of an unmanned aircraft to avoid collision. The network has 5 inputs (encoding the relation of the ownship to an intruder) and 5 outputs (corresponding to actions: weak left, weak right, strong left, strong right, and clear-of-conflict). Given an input, the network advises the action assigned the lowest value. Proving that the network does not produce erroneous advisories is paramount for ensuring the safe operation of the aircraft. We consider four realistic, desirable properties for each of the 45 networks. These properties, numbered 1–4, are taken from [14].

**TaxiNet Family** The TaxiNet family contains perception networks used in vision-based *road-following*: the task of predicting the position of an aircraft on the taxiway relative to the center-line, so that a controller can accurately adjust the position of the aircraft [6]. The input to the network is a grey-scale image of the runway captured from a wing of the aircraft. The network produces two outputs, the lateral distance to the runway center-line, and the heading angle error with respect to the center-line. Proving that the networks accurately predict the location of the aircraft even when the camera image suffers from small noise (e.g., tire skid marks) is safety-critical. This property can be captured as local adversarial robustness and written as a VNN formula. For instance, if the  $k^{\text{th}}$  output of the network is expected to be  $b_k$  for inputs near  $\mathbf{a}$ , we can check if the following formula is satisfiable:

$$(y_k \geq b_k + \epsilon) \wedge \bigwedge_{i=1}^N (a_i - \delta \leq x_i \leq a_i + \delta),$$

where  $\mathbf{x}$  denotes the actual network input, and  $y_k$  denotes the actual  $k^{\text{th}}$  output. The network is  $(\delta, \epsilon)$ -locally robust on input  $\mathbf{a}$ , only if the formula is unsatisfiable.

The training data comes from the X-Plane 11 simulator. To achieve different network sizes, the training images are compressed, to either 2048 (64x32) or 512 (32x16) pixels. We evaluate the local adversarial robustness of two networks with different architectures. The first, TaxiNet1, has 2048 inputs, 1 convolutional layer and 128 relus. The second, TaxiNet2, has 512 inputs, 5 convolutional layers, and a total of 176 relus. For each network, we generate 100 local adversarial robustness queries concerning the first output (distance to the center line).

For each model, we sample 100 uniformly random images from the training data, and sample  $(\delta, \epsilon)$  pairs uniformly from the set  $\{\langle 0.004, 3 \rangle, \langle 0.004, 9 \rangle, \langle 0.008, 3 \rangle, \langle 0.008, 9 \rangle, \langle 0.016, 9 \rangle\}$ . Setting  $\delta = 0.004$  allows a 0.4% perturbation in pixel brightness, and the units of  $\epsilon$  are meters.

**MNIST** In addition to the two neural network families with safety-critical real-world applications, we evaluate our techniques on three fully-connected feed-forward neural networks (MNIST1, MNIST2, MNIST3) trained on the MNIST dataset [21] to classify hand-written digits. Each network has 784 inputs (representing a 28x28 grey-scale image) with value range  $[0, 1]$ , and 10 outputs (each representing a digit). MNIST1 has 10 hidden layers and 10 neurons per layer; MNIST2 has 10 hidden layers and 20 neurons per layer; MNIST3 has 20 hidden layers and 20 neurons per layer. Given an input image, the network classifies it as the digit corresponding to the output with the highest score.

For the MNIST networks, we consider *targeted robustness*. Targeted robustness queries ask whether, for an input  $\mathbf{x}$  and an incorrect output  $y'$ , there exists a point

in the  $\ell^\infty$   $\delta$ -ball around  $x$  that is classified as  $y'$ . We sample 100 targeted robustness queries for each network, by choosing random training images and random incorrect labels. We choose  $\delta$  values evenly from  $\{0.004, 0.008, 0.0016, 0.0032\}$ .

## 4.2 Implementation

We implemented the techniques proposed above in the open-source Marabou neural network verificaiton tool [16]. In this section, we refer to Marabou running the D&C algorithm as D&C-Marabou. Two partitioning strategies are supported: the original input-based partitioning strategy<sup>8</sup> and our new ReLU-splitting strategy. All D&C configurations use the following parameters: the initial partition size  $N_0$  is the number of available processors; the initial timeout  $T_0$  is 40% of the network size in seconds; the number of online partitions  $N$  is 4; and the timeout factor  $F$  is 1.5. The parameters were chosen using a grid search on a small subset of benchmarks. The question of more fine-grained parameter selection is left to future work.

**Tree-state restoration** The **partition** function yields sub-problems that differ in only a small subset of their constraints, resulting in similar work being done in all sibling problems. Some of this can be avoided by storing the state of Marabou after initial bound propagation and before search begins. Should a formula  $\phi$  timeout, rather than starting from scratch, we add the constraints created from partitioning to their parent’s stored state. This straightforward implementation generally reduces runtime and is therefore on by default.

## 4.3 Experimental results

We present the results of the following experiments:

1. Evaluation of each technique’s effect on run time performance of Marabou on the ACAS Xu, MNIST, and TaxiNet benchmarks. We also compare against Neurify, a state-of-the-art solver, on a subset of benchmarks that it admits.
2. An analysis of trade-offs when running iterative propagation pre-processing.
3. Exploration of D&C scalability at a large scale, using cloud computing.

**Evaluation of the techniques on ACAS Xu, MNIST, TaxiNet** We denote the ReLU-based partitioning strategy as **R**, polarity-based direction heuristics as **D**, and iterative propagation as **P**. We run four combinations of our techniques: 1. **R**; 2. **R+D**; 3. **R+P**; and 4. **R+D+P**, and compare them with two baseline configurations: 1. the sequential mode of Marabou (denoted as **M**); 2. D&C Marabou with its default input-based partitioning strategy (denoted as **I**). The  $k$  parameter for the direction heuristic (see Section 3.2) is set to 5, and the timeout for each ReLU during iterative propagation is set to 2 seconds.

We run all six Marabou configurations on the entire benchmark set on a cluster equipped with Intel Xeon E5-2620 v4 cpus running Ubuntu 16.04. 8 processors, 64GB RAM are allocated for each job, except for the **M** configuration, which uses 1 processor and 8GB RAM per job. Each job is given an 1-hour wall-clock timeout.

<sup>8</sup> We use the version of this strategy implemented in the latest version of Marabou, which differs from the one reported in [16]. In particular, the current version splits on the input variable with the widest bounds. We found that the performance of this heuristic on the ACAS Xu benchmarks is competitive with the old one.

Subset	<b>M</b>		<b>I</b>		<b>R</b>		<b>R+D</b>		<b>R+P</b>		<b>R+D+P</b>	
#	S	T	S	T	S	T	S	T	S	T	S	T
ACAS1	0	0	0	0	0	0	0	0	0	0	0	0
	45	0	0	7 13745	7	16666	<b>10 23247</b>	6	13516	10	24331	
ACAS2	21	24566	37	15029	36	17625	36	12377	<b>38 20369</b>	37	15090	
	45	0	0	1 3158	1	3311	<b>1 2102</b>	1	3062	1	2316	
ACAS3	<b>3</b>	<b>24</b>	3	26	3	35	3	29	3	417	3	390
	45	35 22431	38	16469	41	21669	<b>42 17739</b>	41	21718	42	23353	
ACAS4	<b>3</b>	<b>18</b>	3	28	3	33	3	29	3	318	3	291
	45	39 19172	40	9283	42	17797	<b>42 11037</b>	40	17089	41	17617	
<b>ACAS</b>	27	24608	43	15083	42	17693	42	12435	<b>44 21104</b>	43	15771	
	180	74 41603	86	42655	91	59443	<b>95 54125</b>	88	55385	94	67617	
MNIST1	14	6146	15	7343	18	6222	17	2275	18	5672	<b>19</b>	<b>7414</b>
	100	61 17789	42	4727	69	20404	71	18786	71	20113	<b>71</b>	<b>18322</b>
MNIST2	1	237	3	3777	4	3846	<b>5 2025</b>	3	1364	5	4290	
	100	37 25676	23	10944	44	26709	<b>53 24331</b>	53	27616	53	25333	
MNIST3	1	223	1	1474	2	4996	<b>3 4236</b>	1	1975	3	5345	
	100	42 20716	23	15142	48	37428	<b>55 29832</b>	54	49103	55	48349	
<b>MNIST</b>	16	6606	19	12594	24	15064	25	8536	22	9011	<b>27</b>	<b>17853</b>
	300	140 64181	88	30813	161	84541	<b>179 72949</b>	178	96832	179	92004	
TaxiNet1	10	1433	10	3719	10	563	<b>10 487</b>	10	945	10	611	
	100	76 13627	58	8831	84	26505	88 25534	87	29019	<b>90</b>	<b>32023</b>	
TaxiNet2	22	1665	22	148	<b>24 4564</b>	23	3287	22	542	23	3665	
	100	52 6821	43	8828	51	4895	53 13014	<b>58 539</b>	58	735		
<b>TaxiNet</b>	32	3098	32	3867	<b>34 5127</b>	33	3774	32	1487	33	4276	
	200	128 20448	101	17659	135	31400	141 38548	145 29558	<b>148 32758</b>			
<b>All</b>	75	34312	94	31544	100	37884	100	24745	98	31602	<b>103</b>	<b>37900</b>
	680	342 126232	275	91127	387	175384	415 165622	411 181775	<b>421 192379</b>			

Table 1: Number of solved instances (S) and run time in seconds (T) of different configurations. For each family, top and bottom rows show data for satisfiable (SAT) and unsatisfiable (UNSAT) instances respectively.

Table 1 shows a detailed breakdown of the number of solved instances and run time of the six configurations across all benchmark sets. We break down the ACAS Xu benchmarks by properties, while breaking down the MNIST and TaxiNet benchmarks by network architectures. We decompose the results by SAT and UNSAT instances. For each row, we highlight the entries corresponding to the configuration that solves the most instances (ties broken by run time). The key observations are:

1. D&C Marabou with ReLU-splitting (**R**) already outperforms the two baseline configurations on most benchmark sets. Moreover, it solves more instances than **I** on the ACAS benchmarks, suggesting that ReLU-splitting is competitive even for low-dimensional input spaces.
2. The polarity-based heuristic and iterative propagation each improve the overall performance of D&C-Marabou. Interestingly, the polarity-based heuristic improves the performance on not only SAT but also UNSAT instances. This suggests that by affecting how ReLU constraints are repaired, direction heuristics also favorably impact the order of relu-splitting in Marabou (recall from Section 2 that the Reluplex procedure lazily splits on a ReLU if the number of

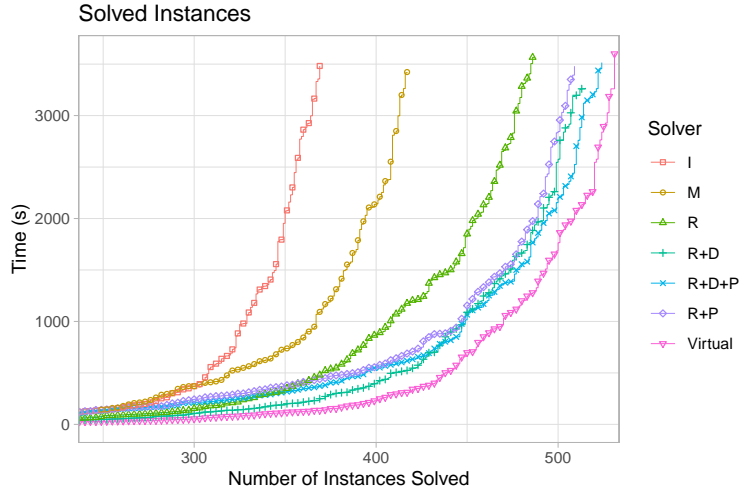


Fig. 6: Cactus plot of all configurations plus the virtual best configuration.

times it is broken reaches a predefined threshold). On the other hand, iterative propagation alone only seems to improve performance on UNSAT instances.

3. **R+D+P** solves the most instances among all the configurations, indicating that the polarity-based direction heuristics and iterative propagation are complementary to each other. In particular, the disadvantage of iterative propagation on SAT instances seems to be mitigated, and the advantage of both techniques on UNSAT instances seems to be amplified.

Figure 6 shows a cactus plot of the 6 configurations on all benchmarks. In this plot, we also include a virtual portfolio configuration that takes the best run time among all configurations for each instance. One particularly interesting point to notice here is that **R+P** is outperformed by **R** in the beginning but surpasses **R** after 500 seconds. A similar pattern can be observed between the trajectory of **R+D** and **R+D+P**. This suggests that iterative propagation creates overhead for easy instances, but benefits the search in the long run.

Figure 7 is a comparative illustration of solver runtime on all benchmarks. The bottom left plot compares our best configuration, **R+D+P**, with the configuration that strips away iterative propagation. The plot shows that iterative propagation is especially effective on the TaxiNet1 benchmarks, contributing to a more than 8x speed-up on many instances. The top right figure demonstrates the effect of the direction heuristics: they produce a modest but significant speedup on many instances. The top left compares the ReLU-based partitioning strategy, **R**, with the input-based partitioning strategy, **I**. **I** is competitive on the ACAS benchmarks but performs consistently worse on perception networks (which have a larger number of inputs). Finally, the bottom right figure shows the performance gain by all of the parallelization techniques compared with the sequential version of Marabou. With 8 processors, we achieve more than 4x speed up on a large portion of benchmarks.

**Comparison with State-of-the-Art** We compare our system with the state-of-the-art solver Neurify. Since Neurify does not support the targeted attack queries of our MNIST benchmarks and since we could not get it to parse our TaxiNet

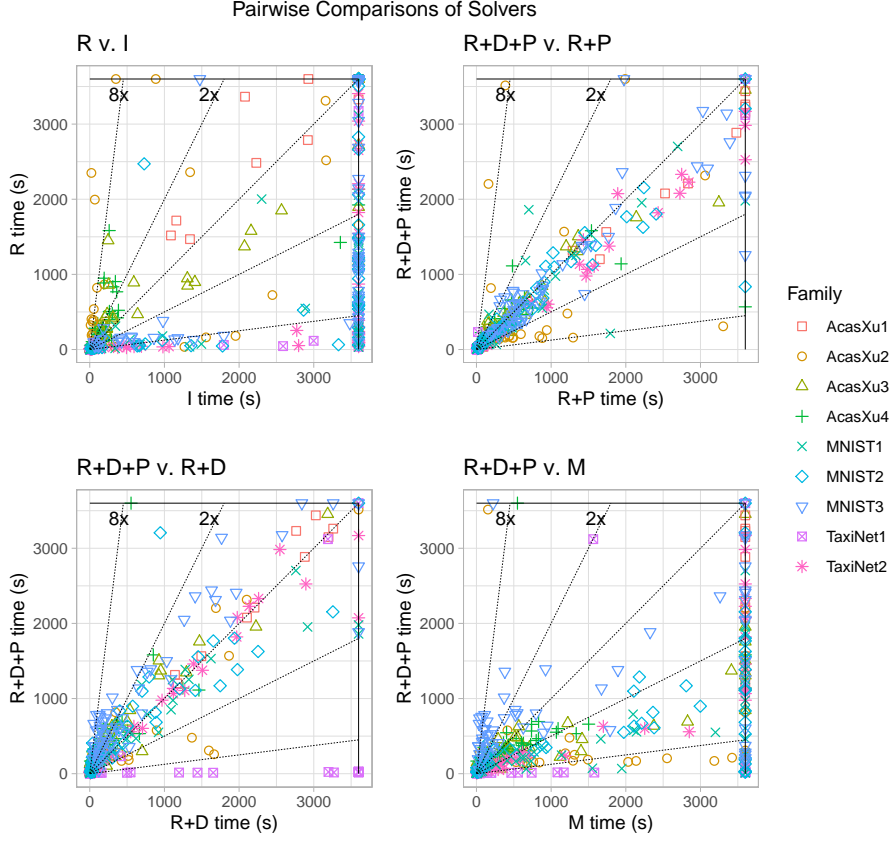


Fig. 7: Pairwise comparison between different configurations on all benchmarks.

networks, we evaluate it on the 180 ACAS Xu benchmarks. We use the same experimental environment described above (8 processors, 64GB RAM, and 1 hour timeout). Like D&C Marabou, Neurify supports parallelization based on input-region partitioning on the ACAS Xu benchmarks.

As shown in Table 2, despite our improvements, Marabou still cannot compete with Neurify on proving UNSAT. However, Marabou can solve more SAT instances within the timeout. We conjecture that one reason Neurify is efficient in proving UNSAT is that it uses sophisticated bound-tightening techniques such as linear relaxation and directed constraint refinement [31]. These techniques could potentially be integrated into Marabou, and are compatible with D&C.

	R+D+P		Neurify	
	S	T	S	T
SAT	43	15771	38	1548
¬SAT	94	67617	133	2032

Table 2: Comparison between D&C and Neurify on the ACAS Xu benchmarks.

**Costs of Iterative Propagation** As mentioned in Sec. 2, intuitively, the longer the time budget during iterative propagation, the more ReLUs should get fixed. To investigate this trade-off between the number of fixed ReLUs and the overhead, we choose a smaller set of benchmarks (40 Acas Xu benchmarks, 40 MNIST benchmarks, and 40 TaxiNet benchmarks), and vary the timeout parameter  $t$  of iterative propagation. Each job is run with 32 cores, and a wall-clock timeout of 1 hour.

Timeout per ReLU(s)	1	2	4	8	16
Mean % of fixed ReLUs	20.4%	21%	22.6%	27.2%	29.8%
Mean wall-clock time(s)	22	31	49	79	128

Table 3: Result of Iterative Propagation with different timeouts.

Table 3 shows the average percentage of fixed ReLUs, and the average wall-clock time of iterative propagation on a formula. As expected, the longer we invest in iterative propagation, the more ReLUs it is able to fix. Each configuration solves the same 106 benchmarks out of 120, except for timeout=16, which solves one more. Figure 8 shows the preprocessing time + solving time of different configurations on commonly solved instances. Though the solving time continues to decrease as we invest more in iterative propagation, performing iterative propagation no longer provides performance gain on these benchmarks when the timeout per ReLU exceeds 8 seconds.

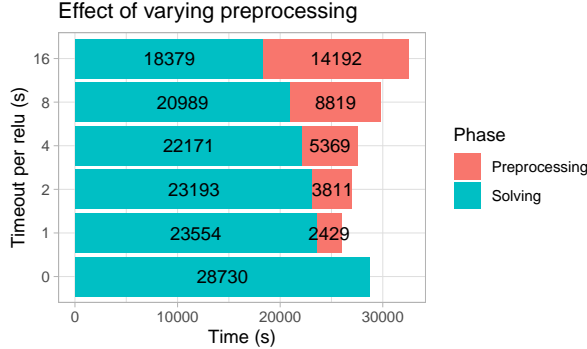


Fig. 8: The effect of varying per-ReLU timeout in preprocessing.

**Ultra-Scalability of D&C** D&C-Marabou runs on a single machine, which intrinsically limits its scalability to the number of hardware threads. To investigate how the D&C algorithm scales with much higher degrees of parallelism, we implemented it on top of the **gg** platform.

The **gg** platform is a tool for expressing parallelizable computations and executing them. To use it, the programmer expresses their computation as *task graph*: a dependency graph of tasks, where each task is an executable program (e.g., a binary or shell script) that reads some input files and produces some output files. These output files can encode the result of the task, or an extension to the task graph that must be executed in order to produce that result. The **gg** platform includes tools for executing tasks in parallel. Tasks can be executed *locally*, using different pro-

cesses, or *remotely*, using cloud services such as AWS Lambda.<sup>9</sup> Since these cloud services offer a high degree of concurrency with little setup or administration, `gg` is a convenient tool for executing massively parallel computations [5].

In our implementation of the D&C algorithm on top of `gg`, each task starts by running the base solver. If the result is `SAT` or `UNSAT`, then this solution is returned by the task. If the base solver times out, the task instead divides its query into sub-queries, and returns a task graph extension containing them. We call this implementation of the D&C algorithm on top of `gg`, “`gg`-Marabou”.

We measure the performance of D&C-Marabou and `gg`-Marabou at varying levels of parallelism to establish that they perform similarly and to demonstrate the scalability of the D&C algorithm. We answer two questions:

- Is `gg`-Marabou significantly slower than D&C-Marabou? That is, does `gg` introduce significant overhead? (*No.*)
- Can the D&C algorithm scale to hundreds of workers? (*Yes.*)

Our experiments use three underlying infrastructures: D&C-Marabou (denoted `thread`), `gg`-Marabou executed locally using OS processes (denoted `gg-local`), and `gg`-Marabou executed remotely on AWS Lambda (denoted `gg-lambda`). We varied the parallelism level from 4 to 16 for the local infrastructures and from 4 to 1000 for the remote infrastructures<sup>10</sup>. For each configuration, we did at least 3 runs per benchmark, discarding any outliers.<sup>11</sup> From the `UNSAT` ACAS benchmarks that D&C-Marabou could solve in under an hour using 4 cores, we use the 5 instances that took the longest. We set the initial timeout to 5 seconds, the timeout factor to 1.5, and the online partition count to 4, and use the input-based partitioning strategy (the `I` solver). Figure 9 shows the results.

Our first conclusion from Figure 9 is that `gg` does **not** introduce substantial overhead. At equal parallelism levels, the `gg` infrastructures actually do slightly better than `thread`, likely because `gg`-Marabou runs the solver’s start-up preprocessing on every task, instead of just once. `gg-local` does slightly better than `gg-lambda`, likely because `gg-lambda` requires network communication.

Our second conclusion is that `gg`-Marabou continues to scale well up to hundreds of workers. This is shown by the constant slope of the runtime/parallelism level line up to  $\sim 512$  workers. We note that the slope only flattens when total runtime is small: about one minute.

## 5 Related Work

Over the past few years, several tools have been developed for verifying neural networks. Most of these tools are sequential in nature, however. In fact, to our knowledge, only Marabou [16] and Neurify [31] (and its predecessor ReluVal [30]) leverage parallel computing to speed up verification. Marabou is an open-source

<sup>9</sup> AWS Lambda is a *serverless* cloud service: one which allows customers to rent a stateless server to execute some computation, paying only for the time spent on the computation.

<sup>10</sup> These limits are imposed by our test machine and AWS Lambda respectively.

<sup>11</sup> Some runs took hundreds of seconds longer than others with the same configuration when using the `gg-lambda` infrastructure. We believe these outliers are caused by AWS Lambda itself, and do not reflect the scalability of the D&C algorithm.

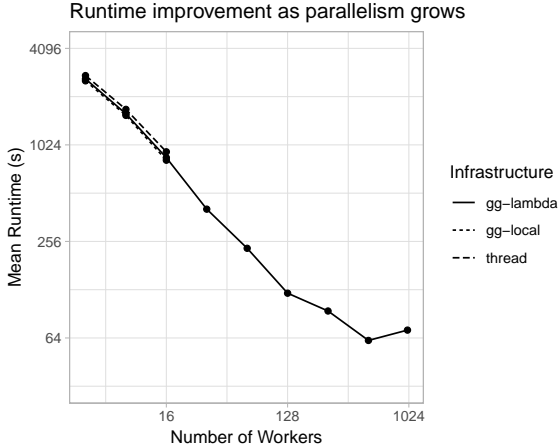


Fig. 9: Scalability of the input splitting strategy. The “Mean Runtime” is over trials and then benchmarks.

implementation of the Reluplex calculus [14] (described in Section 2). It supports parallel solving based on divide-and-conquer with interval-splitting and forms the baseline for the work in this paper.

Neurify [31] builds upon ReluVal [29] by combining symbolic interval analysis with linear relaxation to compute tighter output bounds, and by employing a technique called directed constraint refinement, wherein off-the-shelf solvers are used to handle nodes whose bounds are potentially over-estimated. These interval analysis techniques lend themselves well to parallelization as independent linear programs can be created and checked in parallel. In comparison, we create partitions and solve them in parallel. Furthermore, the architecture of Neurify limits the types of networks and properties it can support, whereas our tool can support any network and property expressible as a VNN formula.

Our work is inspired by the *Cube-and-Conquer* work [9], which targets very hard SAT problems. Cube-and-Conquer is a divide-and-conquer technique that partitions a Boolean satisfiability problem into sub-problems by conjoining cubes—a cube is a conjunction of propositional literals—to the original problem and then employing a conflict-driven SAT solver [26] to solve each sub-problem in parallel. The propositional literals used in cubes are chosen using look-ahead [10] techniques. Our approach uses similar ideas but in a different domain.

## 6 Conclusions and Future Work

In this paper, we presented a set of techniques that leverage parallel computing to improve the scalability of neural network verification. We described an algorithm based on partitioning the verification problem in an iterative manner and explored two strategies that work by partitioning the input space or by splitting on ReLUs, respectively. We also introduced a highly parallelizable pre-processing algorithm for simplifying neural network verification problems. Our experimental evaluation shows the benefit of these techniques on existing and new benchmark. A preliminary

nary experiment with ultra-scaling using the gg platform on Amazon Lambda also showed promising results.

Future work includes: (1) Investigating more dynamic strategies for choosing hyper-parameters of the D&C framework. (2) Investigating the scalability of ReLU-based partitioning on the gg platform. (3) Improving the performance of the underlying solver, Marabou, by integrating conflict analysis (as in CDCL SAT solvers and SMT solvers) and more advanced bound propagation techniques such as those used by Neurify.

## References

- [1] C. W. Barrett, C. L. Conway, M. Deters, L. Hadarean, D. Jovanovic, T. King, A. Reynolds, and C. Tinelli. CVC4. In *CAV*, volume 6806 of *Lecture Notes in Computer Science*, pages 171–177. Springer, 2011.
- [2] M. Cissé, Y. Adi, N. Neverova, and J. Keshet. Houdini: Fooling deep structured prediction models. *CoRR*, abs/1707.05373, 2017.
- [3] L. M. de Moura and N. Bjørner. Z3: an efficient SMT solver. In *TACAS*, volume 4963 of *Lecture Notes in Computer Science*, pages 337–340. Springer, 2008.
- [4] R. Ehlers. Formal verification of piece-wise linear feed-forward neural networks. In *International Symposium on Automated Technology for Verification and Analysis*, pages 269–286. Springer, 2017.
- [5] S. Fouladi, F. Romero, D. Iter, Q. Li, S. Chatterjee, C. Kozyrakis, M. Zaharia, and K. Winstein. From laptop to lambda: Outsourcing everyday jobs to thousands of transient functional containers. In *2019 USENIX Annual Technical Conference, USENIX ATC 2019, Renton, WA, USA, July 10-12, 2019*, pages 475–488, 2019.
- [6] E. Frew, T. McGee, ZuWhan Kim, Xiao Xiao, S. Jackson, M. Morimoto, S. Rathinam, J. Padial, and R. Sengupta. Vision-based road-following using a small autonomous aircraft. In *2004 IEEE Aerospace Conference Proceedings (IEEE Cat. No.04TH8720)*, volume 5, pages 3006–3015 Vol.5, March 2004.
- [7] I. Goodfellow, Y. Bengio, and A. Courville. *Deep Learning*. MIT Press, 2016. <http://www.deeplearningbook.org>.
- [8] D. Gopinath, H. Converse, C. Pasareanu, and A. Taly. Property inference for deep neural networks. In *2019 34th IEEE/ACM International Conference on Automated Software Engineering (ASE)*, pages 797–809, Nov 2019.
- [9] M. Heule, O. Kullmann, S. Wieringa, and A. Biere. Cube and conquer: Guiding CDCL SAT solvers by lookaheads. In *Haifa Verification Conference*, volume 7261 of *Lecture Notes in Computer Science*, pages 50–65. Springer, 2011.
- [10] M. Heule and H. van Maaren. Look-ahead based SAT solvers. In *Handbook of Satisfiability*, volume 185 of *Frontiers in Artificial Intelligence and Applications*, pages 155–184. IOS Press, 2009.
- [11] M. J. H. Heule, O. Kullmann, and V. W. Marek. Solving and verifying the boolean pythagorean triples problem via cube-and-conquer. In *SAT*, volume 9710 of *Lecture Notes in Computer Science*, pages 228–245. Springer, 2016.
- [12] G. Hinton, L. Deng, D. Yu, G. E. Dahl, A.-r. Mohamed, N. Jaitly, A. Senior, V. Vanhoucke, P. Nguyen, T. N. Sainath, et al. Deep neural networks for acoustic modeling in speech recognition: The shared views of four research groups. *IEEE Signal processing magazine*, 29(6):82–97, 2012.
- [13] K. D. Julian, M. J. Kochenderfer, and M. P. Owen. Deep neural network compression for aircraft collision avoidance systems. *Journal of Guidance, Control, and Dynamics*, 42(3):598–608, 2019.

- [14] G. Katz, C. Barrett, D. Dill, K. Julian, and M. Kochenderfer. Reluplex: An Efficient SMT Solver for Verifying Deep Neural Networks. In *Proc. 29th Int. Conf. on Computer Aided Verification (CAV)*, pages 97–117, 2017.
- [15] G. Katz, C. Barrett, D. L. Dill, K. Julian, and M. J. Kochenderfer. Towards proving the adversarial robustness of deep neural networks. *arXiv preprint arXiv:1709.02802*, 2017.
- [16] G. Katz, D. A. Huang, D. Ibeling, K. Julian, C. Lazarus, R. Lim, P. Shah, S. Thakoor, H. Wu, A. Zeljić, et al. The marabou framework for verification and analysis of deep neural networks. In *International Conference on Computer Aided Verification*, pages 443–452, 2019.
- [17] A. Krizhevsky, I. Sutskever, and G. E. Hinton. Imagenet classification with deep convolutional neural networks. In *Advances in neural information processing systems*, pages 1097–1105, 2012.
- [18] A. Krizhevsky, I. Sutskever, and G. E. Hinton. Imagenet classification with deep convolutional neural networks. In *NIPS*, pages 1106–1114, 2012.
- [19] A. Kurakin, I. J. Goodfellow, and S. Bengio. Adversarial examples in the physical world. In *ICLR (Workshop)*. OpenReview.net, 2017.
- [20] A. L. Maas, A. Y. Hannun, and A. Y. Ng. Rectifier nonlinearities improve neural network acoustic models. In *Proc. icml*, volume 30, page 3, 2013.
- [21] The MNIST database of handwritten digits Home Page. <http://yann.lecun.com/exdb/mnist/>.
- [22] V. Nair and G. E. Hinton. Rectified linear units improve restricted boltzmann machines. In *ICML*, pages 807–814. Omnipress, 2010.
- [23] R. Nieuwenhuis, A. Oliveras, and C. Tinelli. Solving sat and sat modulo theories: From an abstract davis–putnam–logemann–loveland procedure to dpll( $t$ ). *J. ACM*, 53(6):937–977, 2006.
- [24] L. Pulina and A. Tacchella. An abstraction-refinement approach to verification of artificial neural networks. In *CAV*, volume 6174 of *Lecture Notes in Computer Science*, pages 243–257. Springer, 2010.
- [25] L. Pulina and A. Tacchella. Challenging SMT solvers to verify neural networks. *AI Commun.*, 25(2):117–135, 2012.
- [26] J. P. M. Silva, I. Lynce, and S. Malik. Conflict-driven clause learning SAT solvers. In *Handbook of Satisfiability*, volume 185 of *Frontiers in Artificial Intelligence and Applications*, pages 131–153. IOS Press, 2009.
- [27] D. Silver, A. Huang, C. J. Maddison, A. Guez, L. Sifre, G. Van Den Driessche, J. Schrittwieser, I. Antonoglou, V. Panneershelvam, M. Lanctot, et al. Mastering the game of go with deep neural networks and tree search. *nature*, 529(7587):484, 2016.
- [28] C. Szegedy, W. Zaremba, I. Sutskever, J. Bruna, D. Erhan, I. J. Goodfellow, and R. Fergus. Intriguing properties of neural networks. In *ICLR (Poster)*, 2014.
- [29] S. Wang, K. Pei, J. Whitehouse, J. Yang, and S. Jana. Efficient formal safety analysis of neural networks. In *Advances in Neural Information Processing Systems 31: Annual Conference on Neural Information Processing Systems 2018, NeurIPS 2018, 3-8 December 2018, Montréal, Canada*, pages 6369–6379, 2018.
- [30] S. Wang, K. Pei, J. Whitehouse, J. Yang, and S. Jana. Formal security analysis of neural networks using symbolic intervals. In *27th {USENIX} Security Symposium ({USENIX} Security 18)*, pages 1599–1614, 2018.
- [31] S. Wang, K. Pei, J. Whitehouse, J. Yang, and S. Jana. Formal security analysis of neural networks using symbolic intervals. In *27th USENIX Security Symposium, USENIX Security 2018, Baltimore, MD, USA, August 15-17, 2018*, pages 1599–1614, 2018.